JOC The Journal of Organic Chemistry

Article

pubs.acs.org/joc

A Computational Study: Reactivity Difference between Phosphine- and Amine-Catalyzed Cycloadditions of Allenoates and Enones

Gou-Tao Huang, Timm Lankau, and Chin-Hui Yu*

Department of Chemistry, National Tsing Hua University, Hsinchu 30013, Taiwan

Supporting Information

ABSTRACT: Allenoates and enones form cyclopentenes via a phosphine-catalyzed [3 + 2] cycloaddition while the amine-catalyzed [2 + 4] cycloaddition yields dihydropyrans or pyrans. The difference between these catalysts is studied with M06-2X/6-31+G* calculations. The addition of the catalyst to the allenoate is the first step in both pathways followed by the reaction with the enone. The formation of the [3 + 2] phosphorus−ylide is exergonic, and hence, the [3 + 2] cycloaddition is kinetically favored over the [2 + 4] addition. Amines do not stabilize [3 + 2] ammonium−ylides. However, electron-withdrawing groups on the enone enable [2 + 4] cycloadditions. The strength of the electron-withdrawing group further controls the α/γ regioselectivity of the [2 + 4] cycloaddition, and the analysis of the HOMO−LUMO interactions explains why only *E*-dihydropyrans from the direct γ-[2 + 4] cycloaddition have been observed in experiments. The quantum calculations further reveal a new path to the α-[2 + 4] product starting with an intermediate Rauhut−Currier reaction. This new path is kinetically favored over the direct amine-catalyzed α-[2 + 4] cycloaddition.

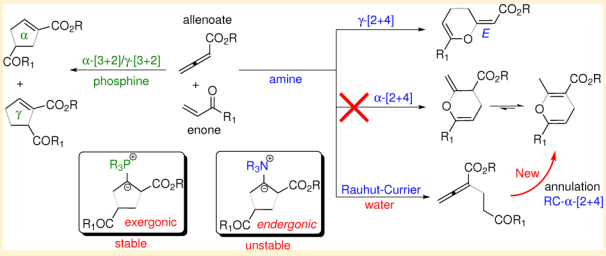

1. INTRODUCTION

Allenes are useful building blocks in the synthesis of many natural products because they are much more reactive than simple alkenes.[1] To access their full synthetic potential, allenic molecules are often activated by Lewis acids or bases. Commonly used Lewis acids for cycloadditions are transition-metal (Rh, Pd, Ni, Mo, Au) complexes,[2−4] while phosphines and nitrogen-based nucleophiles (amines or azaarenes) as Lewis bases have been used to catalyze other types of reactions with allenes.[5]

The [3 + 2] cycloaddition of allenoates and activated alkenes catalyzed by P(*n*-Bu)$_3$ or PPh$_3$ yielding cyclopentene products was first reported in 1995.[6] Asymmetric versions of this reaction have been used for the synthesis of natural products.[7−13] The mechanism originally proposed by Zhang and Lu (Scheme 1) was not verified until 13 years later.[14] The phosphine reacts with the allenic ester to form a zwitterionic PR$_3$·allenoate adduct in the first step. The negative part of the zwitterion resembles an allylic anion, which then reacts with the electron-deficient alkene in an α- or γ-[3 + 2] cycloaddition yielding a five-membered carbocycle with an ylidic $P^{\delta+}$−$C^{\delta-}$ exo bond. A proton transfer initiates the release of the products in the last step. Experiments further showed that the addition of the phosphine to the allenoate is the rate-determining step.[15]

Amines such as 1,4-diazabicyclo[2.2.2]octane (DABCO) or quinuclidine derivatives have been used to catalyze [2 + 4] cycloadditions of allenoates with the enones carrying electron-withdrawing or phenyl groups on the carbonyl carbon atom recently.[16−23] The lower half of Scheme 1 shows the reaction mechanism for the amine catalysis. Similar to the aforementioned phosphine catalysis, the reaction starts with the formation of a zwitterion from the amine and the allenoate. The following γ-[2 + 4] cycloaddition yields the *E*-form dihydropyran product only. However, no [3 + 2] cyclopentene product has been reported in any of the nitrogen-catalyzed reactions.

On the other hand, the Rauhut−Currier reaction (abbreviated as RC, also known as the vinylogous Morita−Baylis−Hillman reaction) has been reported in the amine-catalyzed reaction of allenoates with various enones, such as acrylic esters.[24,25] The reaction starts with the α-Michael addition of the DABCO·allenoate adduct to enones, followed by proton transfer and release of DABCO, to generate linear products, α-substituted allenoates (Scheme 1). Furthermore, α-[2 + 4] pyran products have been observed if electron-poor enones with electron-withdrawing groups are used. Some experiments suggest a link between the RC product (acyclic α-substituted allenoates) and the α-[2 + 4] pyran product.[26,27]

The catalysis with phosphines and amines, though chemically similar, leads to different products from the same reactants. Herein,we investigate the origin of the difference in the catalytic mechanisms. PMe$_3$ and DABCO were chosen as phosphine and amine catalysts in the calculations. This paper is organized as follows. The computational method is described in section 2. The first step of the reaction, which is the addition of the catalysts PMe$_3$/DABCO to the allenoate, is analyzed in section 3.1. The phosphine-catalyzed cycloadditions of the PMe$_3$·allenoate adduct with methyl acrylate (enone **2a**) are discussed in section 3.2, while section 3.3 focuses on the amine-catalyzed reactions of three enones (**2a** and two electron-deficient enones, **2b** and **2c**) to discuss the substituent effect on the catalytic process. The stability of the cyclic [3 + 2] intermediates obtained with

Received: December 2, 2013
Published: January 19, 2014

dx.doi.org/10.1021/jo402609v | J. Org. Chem. 2014, 79, 1700−1711

Scheme 1. Studied Reactions

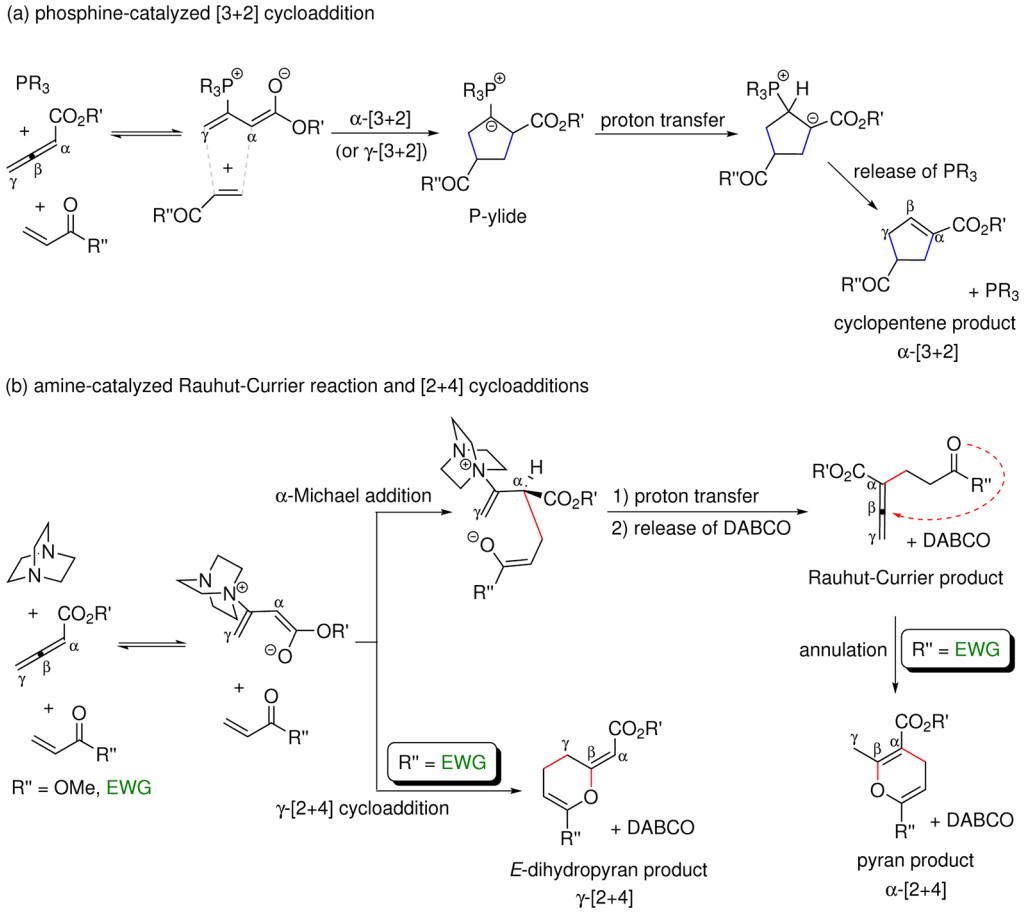

[a]Phosphine-catalyzed [3 + 2] cycloaddition. [b]Amine-catalyzed Rauhut−Currier reaction and [2 + 4] cycloadditions.

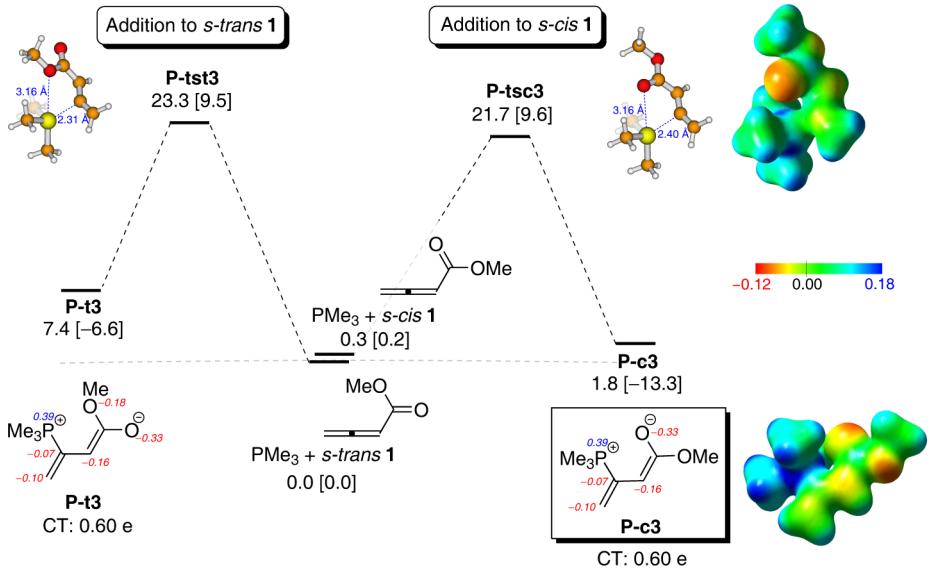

Figure 1. Addition of PMe_3 to methyl allenoate (ΔG [ΔH] in kcal mol^{-1}). Hirshfeld charges (with summing adjacent hydrogen atoms to heavy atoms) and charge transfer (CT) between PMe_3 and allenoates are listed for the adducts **P-c3** and **P-t3**. Electrostatic potential is mapped onto the total electron density isosurface of 0.02.

phosphine and amine catalysts is the subject of section 3.4. Frontier orbitals and electrostatic interactions along both reaction pathways are analyzed in section 3.5. Finally, the conclusion is drawn in section 4.

2. COMPUTATIONAL METHOD

The addition of PMe_3 to methyl allenoate **1** was calculated at M06-2X[28] and single-point CCSD(T)[29] levels in a combination of 6-31+G* and 6-311++G** basis sets (Figure S1, Supporting Information). Besides the

dx.doi.org/10.1021/jo402609v | J. Org. Chem. 2014, 79, 1700−1711

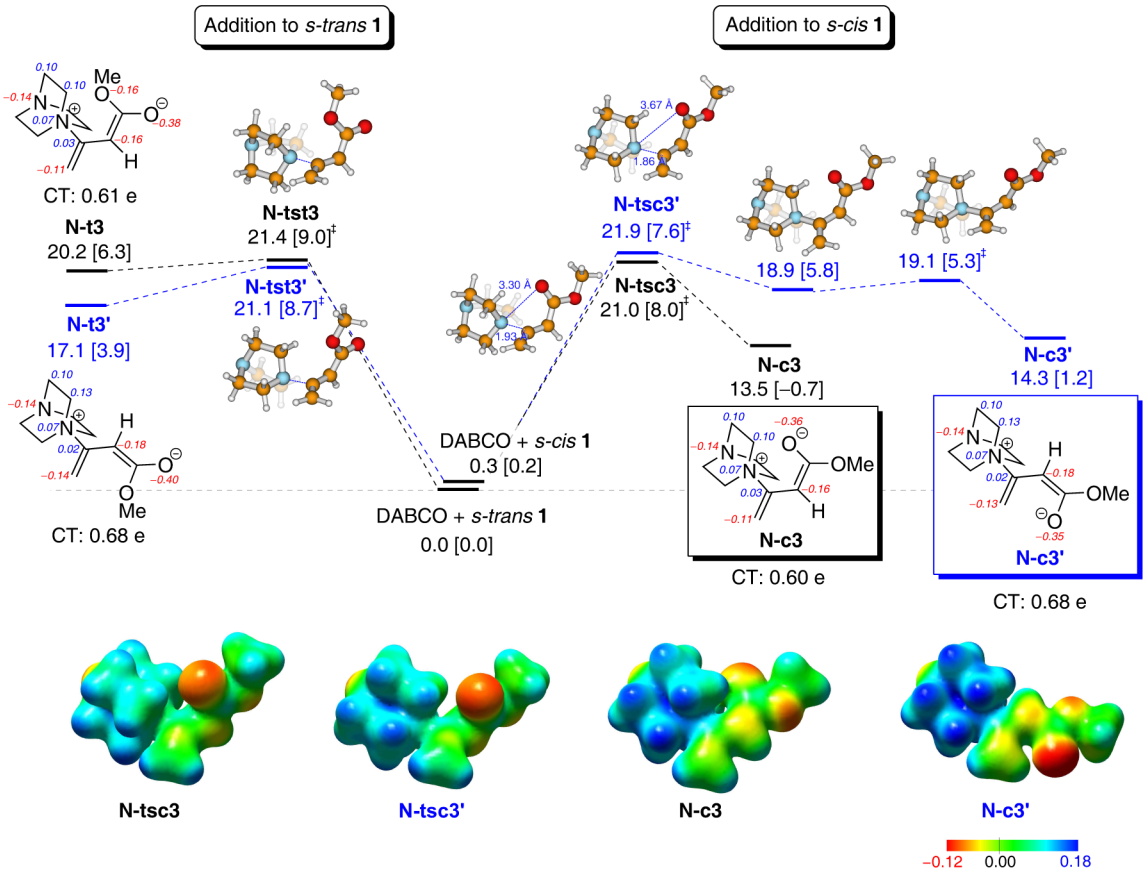

Figure 2. Addition of DABCO to methyl allenoate (ΔG [ΔH] in kcal mol^{-1}). Hirshfeld charges (with summing adjacent hydrogen atoms to heavy atoms) and charge transfer (CT) between DABCO and allenoates are listed for the four adducts, **N-c3**, **N-c3′**, **N-t3**, and **N-t3′**. Electrostatic potential is mapped onto the total electron density isosurface of 0.02.

addition step, all cyclizations for phosphine and amine catalysis were evaluated at the M06-2X/6-31+G* and single-point CCSD(T)/6-31+G* levels (Figures S2 and S3, Supporting Information). The trend obtained from M06-2X/6-31+G* calculations agrees well with that from the high-level CCSD(T) calculations. All calculations presented herein were done at the M06-2X/6-31+G* level as implemented in the Gaussian 09 program suite.[30] All minima and transition states were optimized in the gas phase. Frequencies of the local minima are all positive, and the transition state has one and only one imaginary frequency. The effects of toluene as a solvent were included into the model by the single-point calculations at gas-phase optimized structures with a polarizable continuum model[31−33] (PCM model). All free energy and enthalpy calculations were done on the basis of the PCM frequency calculations assuming 1 atm pressure and a temperature of 298 K. All energies ΔG and ΔH stated here are relative to the separated reactants in toluene. Chemical bonds were analyzed using the electron localization function[34] with the TopMod program by Silvi et al.[35]

3. RESULTS AND DISCUSSION

3.1. Addition of Phosphines and Amines to Allenoates.

All studied reactions start with the addition of the phosphine/amine to the allenoate to form a zwitterionic adduct. Trimethylphosphine and DABCO were chosen as catalysts to react with methyl allenoate **1**. The isomerization of *s-trans* and *s-cis* ethyl allenoate has been observed in NMR experiments.[36] Similar to the experiment, the calculations show that the two isomers of **1** have similar energies ($\Delta\Delta G$ = 0.3 kcal mol^{-1}) with a barrier of 6.8 kcal mol^{-1} for the isomerization.

The addition of PMe_3 to **1** leads to the formation of the adducts **P-c3** and **P-t3** where the '**c**' indicates the *s-cis* allenoate and the '**t**' the *s-trans* isomer (Figure 1). The barrier for the addition of PMe_3 to *s-cis* **1** is 1.6 kcal mol^{-1} smaller than that for the addition to the *s-trans* isomer (**P-tst3**, 23.3 kcal mol^{-1}). The **P-c3** isomer is more stable by 5.6 kcal mol^{-1} in ΔG than **P-t3**.

On the other hand, two transition states (**N-tsc3** and **N-tsc3′**) were localized for the addition of DABCO to *s-cis* **1** yielding the **N-c3** and **N-c3′** adducts, respectively (Figure 2). The DABCO and ester groups are on the same side in **N-c3** and on opposite sides in **N-c3′**. The addition of DABCO to *s-trans* **1** proceeds via a similar pathway to yield the adducts **N-t3** and **N-t3′**. The barriers for the four addition pathways are comparable (~21 kcal mol^{-1}); however, **N-c3** and **N-c3′** are 3−7 kcal mol^{-1} more stable than **N-t3** and **N-t3′**. **N-c3** is the most stable adduct being 13.5 kcal mol^{-1} higher in ΔG than the reactants. The addition of amines to the allenoates is more endergonic than the addition of phosphines.

The Hirshfeld charges[37] of selected atoms in the adducts and the charge transfer (CT) from the catalyst to the allenoate are shown in Figures 1 and 2. The observed charge transfer with both catalysts is similar, 0.60 e with the phosphine and either 0.60 or 0.68 e with DABCO. However, the charge distribution in the linking bonds ($P^{\delta+}$−$C^{\delta-}$ and $N^{\delta+}$−$C^{\delta+}$) is different. The phosphorus atom carries a charge of +0.39 e in **P-c3**, while each methyl group carries +0.07 e. About two-thirds of the positive charge are localized on the phosphorus atom. The analysis of the Hirshfeld charges agrees with that of the electrostatic potential (ESP) map, which also suggests a localization of the positive charge on the phosphorus atom. On the other hand, the linking nitrogen atom in DABCO·allenoate carries only a small charge of +0.07 e. However, each methylene

dx.doi.org/10.1021/jo402609v | J. Org. Chem. 2014, 79, 1700−1711

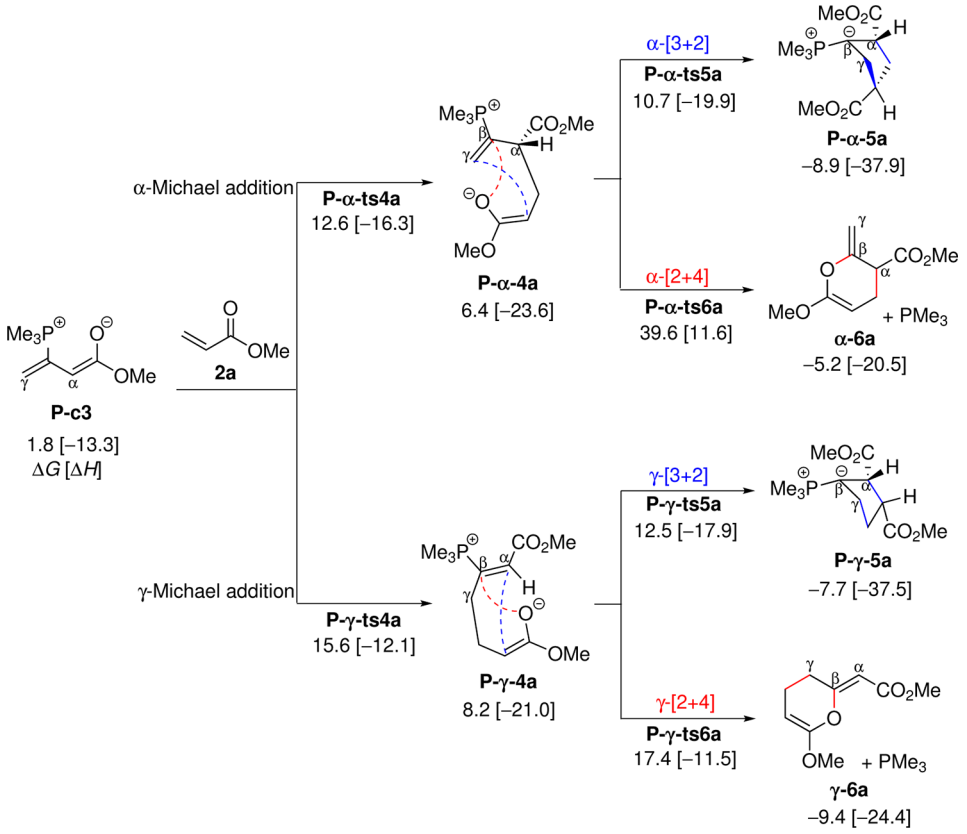

Figure 3. Phosphine-catalyzed [3 + 2] and [2 + 4] cycloadditions starting from **P-c3** and **2a**. Free energies and enthalpies, ΔG [ΔH] in kcal mol^{-1}, are relative to PMe_3, **1** and **2a**.

group carries a charge of +0.10 e or +0.13 e. Hence, a positive charge of approximately +0.64 e is stored in the $-CH_2CH_2-$ groups of DABCO, about nine times more than that on the linking nitrogen atom.

The distribution of the negative charge is nearly the same in all adducts. About −0.35 e are carried by the carbonyl oxygen atom, −0.17 e by C_α and −0.11 e by C_γ. The large negative charge on the carbonyl oxygen atom makes it the primary interaction partner for the positive charge on the catalyst. The strong $P\cdots O_{C=O}$ electrostatic interaction leads to a trigonal bipyramidal coordination of the phosphorus atom in the transition state (**P-tsc3**) and the adduct (**P-c3**) with $P^{0.39}\cdots O^{-0.33}_{C=O}$.[38] The corresponding structures with the weaker $P^{0.39}\cdots O^{-0.18}_{COMe}$ interaction between the phosphorus atom and the ester oxygen atom (**P-tst3** and **P-t3**) are less stable. For amines, the weaker $O\cdots H_2C$ interaction leads to two transition states differing in the number of $O\cdots H_2C$ interactions. One direct interaction can be observed in **N-tsc3′**, while two are observed in **N-tsc3** (Figure 2). Consequently, **N-tsc3** and **N-c3** are slightly lower in energy than **N-tsc3′** and **N-c3′**.

3.2. Phosphine-Catalyzed Cycloaddition. At the beginning of the reaction, the allenoate and the enone compete with each other for the Lewis base catalyst PMe_3. The calculated barrier for the reaction between PMe_3 and enone **2a** is 2.9 kcal mol^{-1} higher than that for the reaction between PMe_3 and the allenoate **1** (see detailed information in Figure S4, Supporting Information). As the formation of the PMe_3·allenoate adduct clearly dominates, the following discussion focuses only on the fate of the PMe_3·allenoate adduct (Figure 3).

Since **P-c3** is more stable than **P-t3**, **P-c3** is chosen for the computation of the reaction with enone **2a**. The α-Michael addition of the α-carbon atom in **P-c3** to **2a** is more favorable than that of the γ-Michael addition ($\Delta G^{\ddagger}$: 12.6 vs 15.6 kcal mol^{-1} in Figure 3). The regioselective formation of a C−C ([3 + 2] ring closure) or a C−O bond ([2 + 4] ring closure) finalizes the cycloaddition in the next step. The [3 + 2] ring closure always has a smaller barrier than the [2 + 4] one. The formation of the phosphine ylides, **P-*α*-5a** and **P-*γ*-5a**, is exergonic by 8.9 and 7.7 kcal mol^{-1} in contrast to the results of previous B3LYP/6-31+G* calculations[14] of the formation of the [3 + 2] ylide being endergonic by 11 kcal mol^{-1}. Our calculations for the change in electronic energy ΔE_{elec} for the ylide formation yield a value of −21.2 kcal mol^{-1} with the B3LYP functional compared to −45.9 kcal mo^{-1} obtained with the M06-2X functional using the same basis set. The corresponding CCSD(T) calculations yield a value of −44.2 kcal mol^{-1}, which suggests that the M06-2X functional performs significantly better in describing the ylide than B3LYP.[39]

The steep drop in free energy associated with the formation of the phosphorus ylide **P-*α* -5a** suggests that the [3 + 2] cyclization step is practically irreversible. The following release of the [3 + 2] cyclopentene products starts with the transfer of the α-proton in **P-*α*-5a**. The two most favorable of the four tested proton-transfer pathways are the self-tautomerization and the H_2O assistance[14,40] routes as shown in Figure 4 (see the detailed information in Figures S14 and S15, Supporting Information) with barriers of 8.7 and 6.7 kcal mol^{-1} relative to **P-*α*-5a**, respectively. The self-tautomerization pathway also implies that the existence of water is not essential for the P-catalyzed [3 + 2] cyclization. The final release of the [3 + 2] cyclopentene product ***α*-5a** is exergonic by 37.7 kcal mol^{-1} relative to separated reactants.

dx.doi.org/10.1021/jo402609v | J. Org. Chem. 2014, 79, 1700−1711

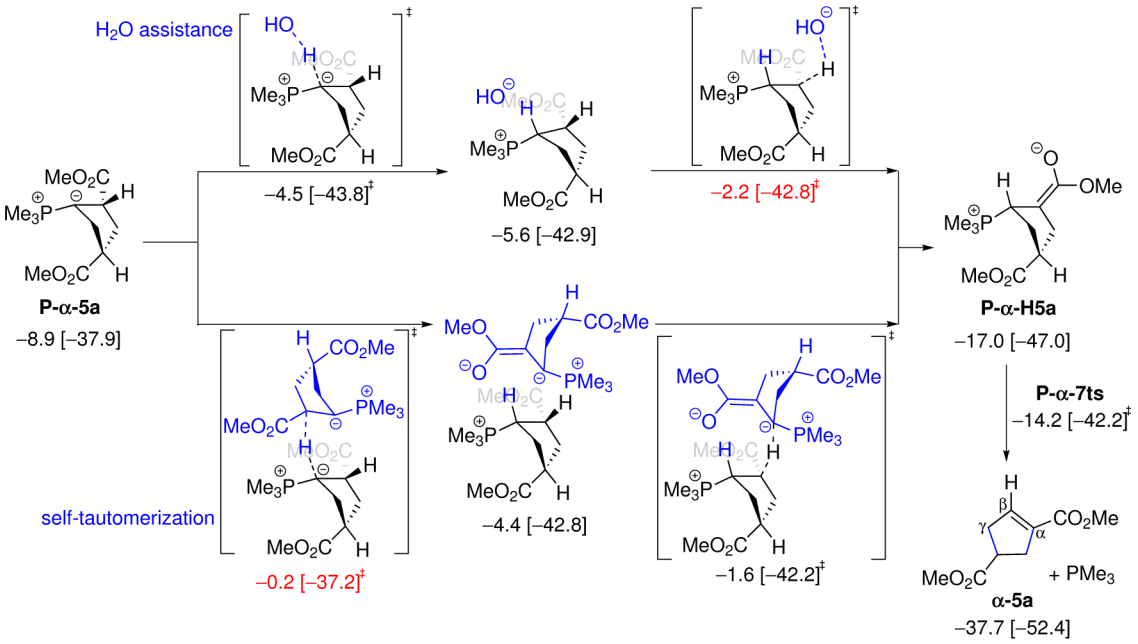

Figure 4. Mechanism of two proton transfer pathways, self-tautomerization, and water assistance. The highest transition-state energies along the two individual pathways are marked in red.

As for the [2 + 4] cycloaddition, the barrier for the γ-[2 + 4] ring closure is higher than that for the C−C ring closure in the γ-[3 + 2] cycloaddition (17.4 vs 12.5 kcal mol^{-1} in Figure 3) but still lower than that for the addition of PMe_3 to **1** (21.7 kcal mol^{-1}). Hence, the γ-[2 + 4] cycloaddition appears to be less favorable than the γ-[3 + 2] addition, although the formation of similar C−O bonds has been observed in other phosphine-catalyzed reactions.[41,42] The α-[2 + 4] cycloaddition has an even higher barrier of 39.6 kcal mol^{-1} for the ring-closure step and is unlikely to contribute to the overall reaction.

In summary, the calculations show that the [3 + 2] cycloadditions are kinetically preferred to the [2 + 4] cycloadditions as observed in the experiments.[6−13] The rate-determining step is the addition of the phosphine to the allenoate ($\Delta G^{\ddagger}$ = 21.7 kcal mol^{-1}), as reported in previous ^{31}P NMR studies.[13,14] The irreversible formation of the phosphorus ylide as an intermediate proceeds via the [3 + 2] ring closure and is finalized by a proton transfer that leads to the release of the cyclopentene products. The catalyst is regenerated in the last step.

3.3. Amine-Catalyzed Reaction. In addition to **2a**, two additional enones (*E*)-methyl 2-oxo-4-phenylbut-3-enoate **2b** and (*E*)-dimethyl cinnamoylphosphonate **2c** are discussed herein to investigate the influence of the enone substitution pattern onto the known regioselectivity of the reaction. Four conformers of the allenoate·DABCO adduct need to be considered as discussed in section 3.1. Of these four conformers, the two conformers **N-c3** and **N-c3′** are more stable than their counterparts **N-t3** and **N-t3′**. Furthermore, among the two conformers **N-c3** and **N-c3′** the barriers for the reactions of **N-c3′** with the three enones, **2a**, **2b**, and **2c**, are 1−4 kcal mol^{-1} lower (Figures S10−S13, Supporting Information) than that with **N-c3**. The study of the amine catalysis hence focuses on the energetic-favored pathways along **N-c3′**.

Enones are known for their reactivity toward amines. The barrier for the formation of the allenoate·DABCO adduct is about 21 kcal mol^{-1} (Figure 2). Initial tests showed that the corresponding barriers for the addition of DABCO to the enones **2a−c** are 18.6, 14.9, and 13.6 kcal mol^{-1} (Figure S5, Supporting Information). The barriers for the addition to the three enones are lower than that for the addition to **1**, but the reverse reaction is nearly barrierless (0.1 to 0.6 kcal mol^{-1}), which makes the formation of the enone·DABCO adduct kinetically labile. Moreover, the barriers for the followup reactions (the addition of the enone·DABCO adduct to the allenoate **1** or the second enone) are over 30 kcal mol^{-1}, and hence, it is possible to neglect any reaction path involving direct adducts of DABCO and the enones. Detailed information about these three reactions is provided in the Supporting Information.

Unlike phosphines, DABCO catalyzes the Rauhut−Currier (RC) reaction[24,25] and the γ-[2 + 4] cycloaddition,[16−19,21−23] which lead to acyclic α-substituted allenoates and cyclic dihydropyrans, respectively. The RC reaction and γ-[2 + 4] cycloaddition are competitive reactions for the same reactants, the allenoate and the enone.

3.3.1. Rauhut−Currier Reaction. The RC reaction starts with the α-Michael addition of **N-c3′** to the enone **2*x*** yielding **N-*α*-4*x*′**, as depicted in Scheme 2, where ***x*** denotes **a**, **b**, or **c**. There are the five possible mechanisms for the proton transfer in the succeeding step: a direct 1,3-proton transfer, a DABCO assistance, an **N-c3′** assistance, a self-tautomerization, and a water assistance (Figures S16 and S17, Supporting Information). Among the five pathways, the H_2O-assisted mechanism was found to be the most efficient one with the lowest activation energy. A similar catalytic effect has been observed in experiments with the Morita−Baylis−Hillman reaction, which is also faster in protic media, such as water.[43−45] The calculations confirm that water is essential to the RC pathway, as mentioned in a previous experiment.[18] The final α-substituted allenoate ***α*-H4*x*** is formed by the release of the DABCO molecule. The activation energies of two critical steps, the α-Michael addition and the protonation on the enolate part of **N-*α*-4*x*′**, are listed in Scheme 2, while detailed information is provided in Figure S18 (Supporting Information). The highest activation energies along the RC pathways with **2a**, **2b**, and **2c** are 27.6, 23.4, and 20.8 kcal mol^{-1}, respectively. Compared to **2a**, the

dx.doi.org/10.1021/jo402609v | J. Org. Chem. 2014, 79, 1700−1711

Scheme 2. Mechanism of the Water-Assisted Rauhut−Currier Reaction[a]

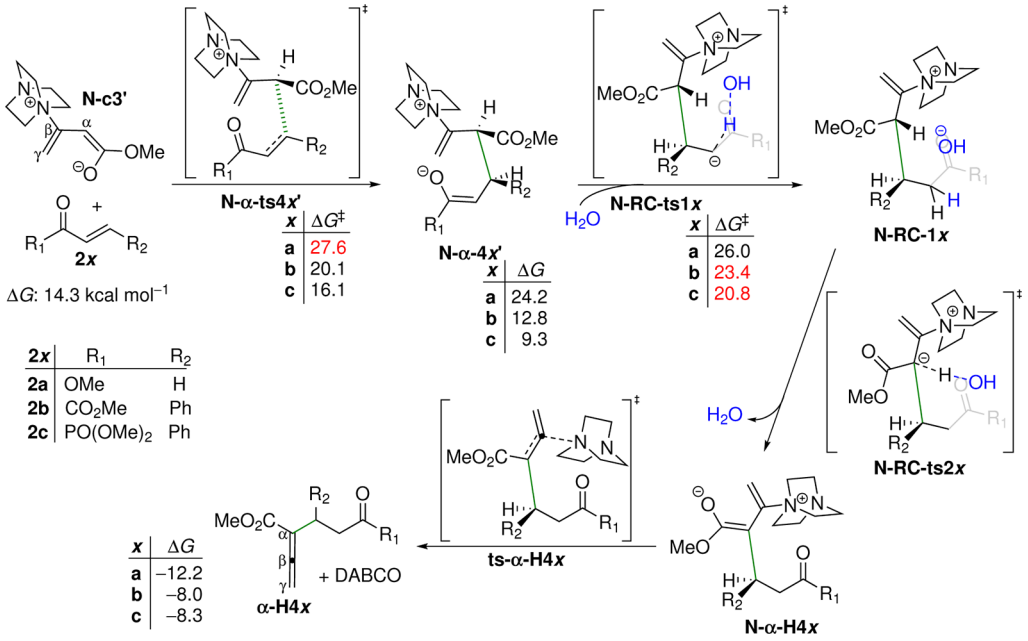

[a]Barriers ($\Delta G^{\ddagger}$ in kcal mol^{-1}) for the α-Michael addition (**N-α-ts4x′**) and the protonation by H_2O (**N-RC-ts1x**) are listed. Red values represent the highest activation energies along the RC pathway of **2a−c**.

Scheme 3. Amine-Catalyzed [3 + 2] and [2 + 4] Cycloadditions

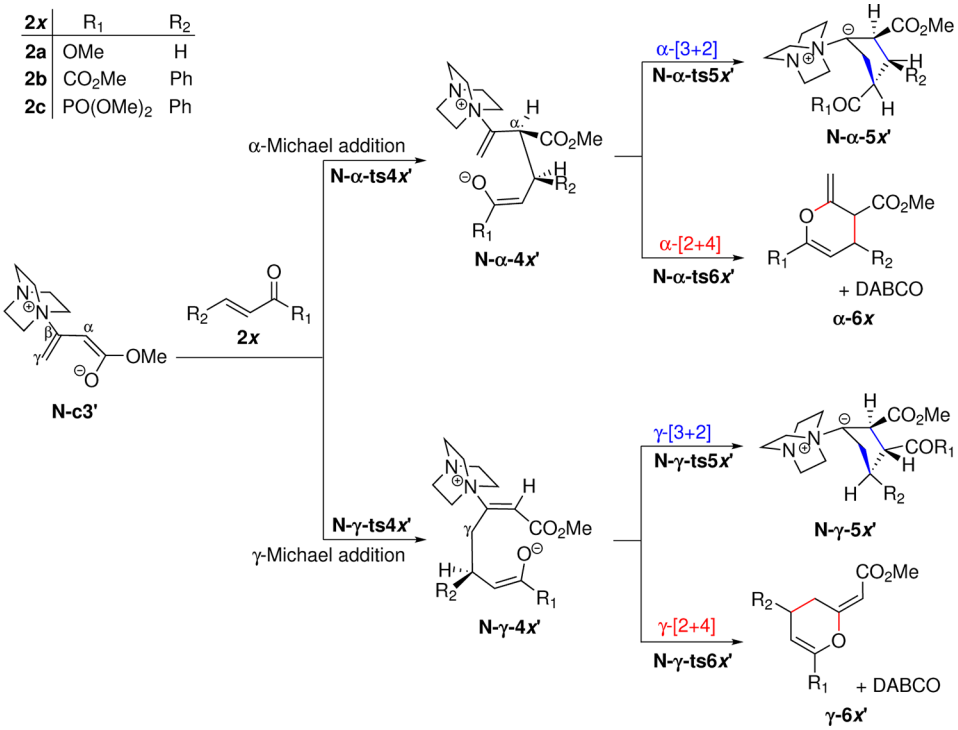

electron-withdrawing substituent in **2b** and **2c** leads to the decrease in the barrier of the α-Michael addition and further stabilizes the enolate part of **N-α-4b′** and **N-α-4c′**, being 12.8 and 9.3 kcal mol^{-1} in ΔG.

3.3.2. Cycloadditions. The mechanisms for the DABCO-catalyzed [3 + 2] and [2 + 4] cycloadditions are illustrated in Scheme 3, and the corresponding energies are summarized in Table 1. The reaction mechanism is similar to that for the phosphine catalysis.

For the acrylic ester **2a**, the barriers for the [3 + 2] and [2 + 4] ring-closure reactions are 29.9 and 47.1 kcal mol^{-1} for the α-addition and 29.2 and 31.7 kcal mol^{-1} for the γ-addition, respectively. The barriers are higher than those for the electron-deficient enones **2b** and **2c**. Hence, enone **2a** is the least reactive one for cyclizations. The data in Table 1 show that the C−O ring closure in the γ-[2 + 4] cycloadditions with **2b** and **2c** has a lower barrier than the γ-Michael addition, whereas the other ring closures are higher in $\Delta G^{\ddagger}$ than their corresponding addition steps. The

dx.doi.org/10.1021/jo402609v | J. Org. Chem. 2014, 79, 1700−1711

Table 1. Energies, ΔG [ΔH] in kcal mol^{-1}, for the [3 + 2] and [2 + 4] Cyclizations in the Cases of 2a−c[a]

		enone 2a		enone 2b		enone 2c	
α-Michael addition	**N-α-ts4x′**	27.6	[−0.9]	20.1	[−8.6]	16.1	[−12.5]
	N-α-4x′	24.2	[−5.3]	12.8	[−15.3]	9.3	[−20.2]
α-[3 + 2] ring closure	**N-α-ts5x′**	29.9	[0.7]	26.3	[−1.6]	23.2	[−5.1]
	N-α-5x′	14.5	[−14.3]	18.6	[−8.6]	18.3	[−10.6]
α-[2 + 4] ring closure	**N-α-ts6x′**	47.1	[16.2]	31.2	[2.3]	31.0	[2.5]
	α-6x	−5.2	[−20.5]	−21.6	[−36.6]	−23.0	[−37.3]
γ-Michael addition	**N-γ-ts4x′**	28.3	[−0.3]	18.8	[−10.4]	16.8	[−13.1]
	N-γ-4x′	21.3	[−8.6]	7.7	[−20.8]	5.2	[−25.1]
γ-[3 + 2] ring closure	**N-γ-ts5x′**	29.2	[0.5]	25.0	[−4.9]	21.7	[−7.6]
	N-γ-5x′	14.1	[−13.9]	16.5	[−11.3]	14.9	[−14.6]
γ-[2 + 4] ring closure	**N-γ-ts6x′**	31.7	[2.0]	14.2	[−14.6]	12.0	[−17.1]
	γ-6x′	−10.3	[−25.2]	−28.0	[−41.4]	−27.4	[−41.4]

[a]All energies are relative to the separated reactants, DABCO, **1**, and **2x**.

Scheme 4. Mechanism of the Annulation of the RC Product Yielding the α-[2 + 4] Product (RC-α-[2 + 4])[a]

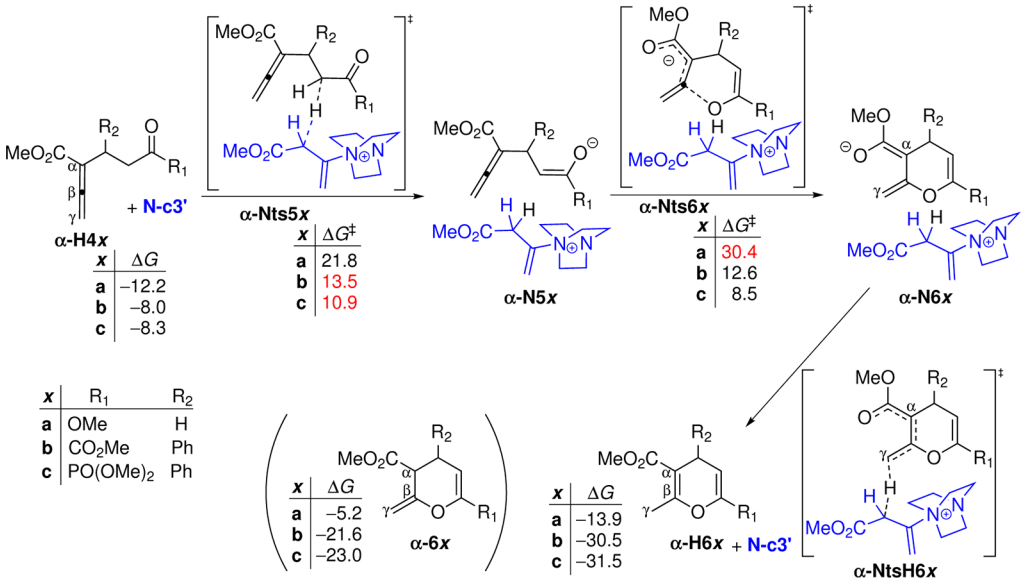

[a]Red values represent the highest activation energies along the annulation pathway of **2a−c**.

γ-[2 + 4] cyclization represents the kinetically favorable reaction pathway ($\Delta G^{\ddagger}$: 18.8 kcal mol^{-1} in **2b**; 16.8 kcal mol^{-1} in **2c**). The formation of the dihydropyran products **γ-6b′** and **γ-6c′** is strongly exergonic by 28.0 and 27.4 kcal mol^{-1}. The calculations indicate that the electron-withdrawing group in **2b** and **2c** speeds up the γ-[2 + 4] cycloaddition, in agreement with the observation that the [2 + 4] cycloaddition of alkenes and enones is accelerated by an electron-withdrawing group on the enone.[46]

Experiments[19] showed that the α-[2 + 4] pyran is the major product if **2c** reacts with **N-c3′**, but the calculations show the γ-[2 + 4] product to dominate as the barrier for the γ-[2 + 4] cycloaddition (16.8 kcal mol^{-1}) is lower than that for the α-[2 + 4] one (31.0 kcal mol^{-1}). Other experiments,[26,27] on the other hand, suggest a link between the RC product and the α-[2 + 4] pyran product. The mechanism of this reaction, denoted as RC-α-[2 + 4], is shown in Scheme 4, where the adduct **N-c3′** acts as a base. The critical barriers along this path associate with the proton abstraction (**α-Nts5x**) and the ring closure (**α-Nts6x**) as the formation of the RC product is practically irreversible. The activation energies of these two steps are listed in Scheme 4. DABCO can also act as a base during the annulation, and the highest barriers for the DABCO-assisted annulation ($\Delta G^{\ddagger}$: 38.4, 20.2, and 15.6 kcal mol^{-1} for **2a**, **2b**, and **2c**, respectively) are significantly higher than those for the **N-c3′**-assisted one ($\Delta G^{\ddagger}$: 30.4, 13.5, and 10.9 kcal mol^{-1} for **2a**, **2b**, and **2c**, respectively). The detailed comparison between **N-c3′** and DABCO acting the bases is provided in Figures S19−S22 (Supporting Information). The resulting pyran **α-H6x** obtained from the γ-protonation of **α-N6x** is about 8 kcal mol^{-1} more stable than **α-6x** from the α-protonation, which is also formed via a direct α-[2 + 4] cycloaddition (Scheme 3). Several studies about the intramolecular ring closure of allenic compounds has shown that the γ-protonated product is more thermodynamically preferred.[47−50] The highest activation energy in the path of the RC reaction with **2c** (Scheme 2) followed by the RC-α-[2 + 4] annulation (Scheme 4) is 20.8 kcal mol^{-1} (**N-RC-ts1c**), which is significantly smaller than a barrier of 31.0 kcal mol^{-1} (**N-α-ts6c′**) for the direct α-[2 + 4] cycloaddition. Similar to **2c**, the α-[2 + 4] pathway via the RC intermediate (**N-RC-ts1b**, $\Delta G^{\ddagger}$ = 23.4 kcal mol^{-1}) is more kinetically facile than the direct α-[2 + 4] cycloaddition with **2b** (**N-α-ts6b′**, $\Delta G^{\ddagger}$ = 31.2 kcal mol^{-1}). Hence, on the basis of barrier heights, it is reasonable to conclude that the observed formation of the α-[2 + 4] product in experiments proceeds through the formation of the RC product as an intermediate.

dx.doi.org/10.1021/jo402609v | J. Org. Chem. 2014, 79, 1700−1711

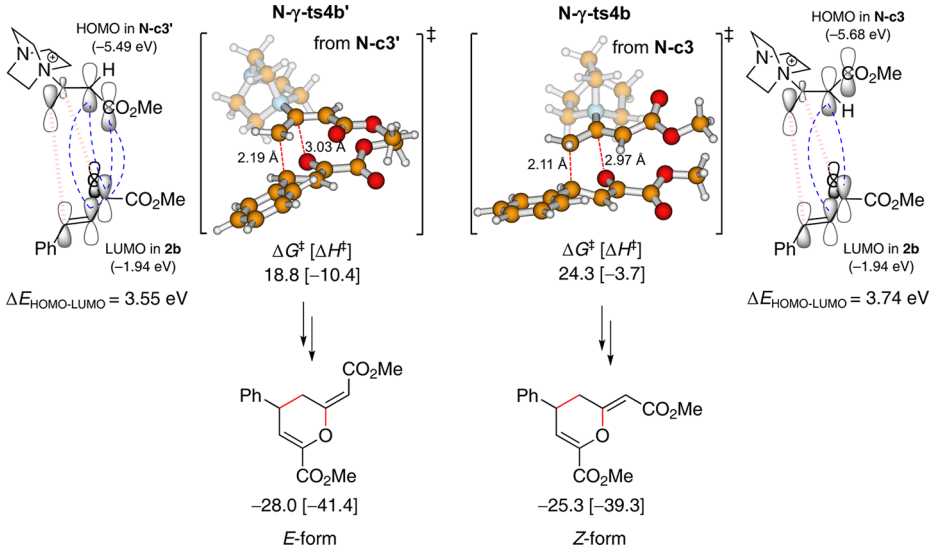

Figure 5. Two transition states of the γ-Michael addition step of **N-c3′**/**N-c3** with **2b** for the γ-[2 + 4] cycloaddition. Activation energies, $\Delta G^{\ddagger}$ [$\Delta H^{\ddagger}$] in kcal mol^{-1}, are relative to DABCO, **1**, and **2b**. The FMO interaction of **N-c3′** and **N-c3** with **2b** is shown.

Even in the cases of enones **2b** and **2c**, the cyclopentene production from the [3 + 2] cycloaddition is seldom observed in experiments.[19] The formation of cyclopentenes results from the cyclopentane ylides **N-α-5b′** or **N-γ-5b′**. Following the α-Michael addition, **N-α-5b′** can proceed along the RC path and the α-[3 + 2] or [2 + 4] ring closure. The RC reaction has the lowest barrier of 23.4 kcal mol^{-1} compared to 26.3 and 31.2 kcal mol^{-1} for the [3 + 2] and [2 + 4] ring closure. Following the γ-Michael addition, **N-α-5b′** undergoes either the [3 + 2] or [2 + 4] ring closure, and the latter is more favorable. The path for **2c** resembles that for **2b**. Therefore, the kinetically disfavored α-[3 + 2] and γ-[3 + 2] cycloadditions explains the absence of the cyclopentene products in the amine-catalyzed reaction.

3.3.3. E/Z Stereoselectivity for γ -[2 + 4] Dihydropyran Products. The *E*-dihydropyran is the major product in the amine-catalyzed γ-[2 + 4] cycloaddition of allenoates and enones.[16−19] The *Z*- and *E*-dihydropyrans result from the cycloaddition of **N-c3** and **N-c3′** with the enones, respectively. The *E*/*Z* stereoselectivity is determined at the γ-Michael addition step, i.e., **N-γ-ts4b′** vs **N-γ-ts4b** (Figure 5), as the γ-Michael addition has a higher activation energy than the C−O ring closure. The barrier for the formation of the *E*-dihydropyran from **N-c3′** and **2b** is 5.5 kcal mol^{-1} lower than that for the corresponding reaction of **N-c3** yielding the *Z*-isomer. Similarly, **N-γ-ts4c′** has a lower activation energy than **N-γ-ts4c** by 4.1 kcal mol^{-1} in the case of enone **2c**.

The analysis of the HOMO−LUMO interactions (Figure 5) is based on the optimized adducts and enones and shows a smaller HOMO−LUMO gap for the *E*-interactions (transition state **N-γ-ts4b′**) than for *Z*-type interactions (transition state **N-γ-ts4b**). The size and sign of the orbital lobes suggest additional bonding overlaps between the allenic −CO_2Me group in the HOMO and the LUMO of the enone in the **N-γ-ts-4b′** transition state. These additional HOMO−LUMO interactions most likely accounts for the preferred formation of *E*-isomers in experiments.

3.3.4. Competition between [2 + 4] Cycloaddition and RC Reaction. In order to discuss the competition between the RC reaction and the γ-[2 + 4] cycloaddition clearly, we summarized critical barriers in Figure 6, where only the highest barriers are given for the macro processes: the addition of DABCO to **1** (I → II), the RC reaction (II → III), the RC-α-[2 + 4] annulation (III → IV) and the α-[2 + 4] cycloaddition (II → V). The detailed steps for the five macro processes, as discussed previously, are omitted in Figure 6.

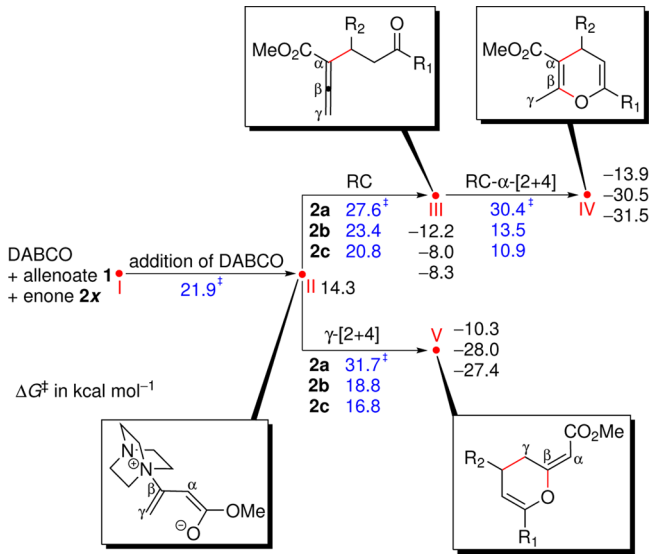

Figure 6. Barriers (blue values) of the rate-determining steps for the addition of DABCO to **1** (I → II), the RC reaction (II → III), the RC-α-[2 + 4] annulation (III → IV) and the γ-[2 + 4] cycloaddition (II → V). All free energies are relative to separated reactants, DABCO, allenoate **1**, and enone **2*x***.

The barrier for the γ-[2 + 4] cycloaddition (31.7 kcal mol^{-1}) is higher than that for the RC reaction (27.6 kcal mol^{-1}) for the least electron-deficient enone **2a**. The α-[2 + 4] annulation starting from the RC product is unfavorable as indicated by a larger activation energy of 30.4 kcal mol^{-1}. The calculations show a clear preference of the RC reaction (I → II → III) for **2a** as observed in experiments.[24,25]

In the case of enone **2b**, the activation energies required for the RC reaction and the γ-[2 + 4] cycloaddition are 23.4 and 18.8 kcal mol^{-1}, respectively, and hence the γ-[2 + 4] cycloaddition (I → II → V) is dominant while the α-[2 + 4] pyran is formed as the minor product from the RC intermediate in the second step (I → II → III → IV), as observed in experiments.[19] In comparison with enone **2a**, the effect of the electron withdrawing

dx.doi.org/10.1021/jo402609v | J. Org. Chem. 2014, 79, 1700−1711

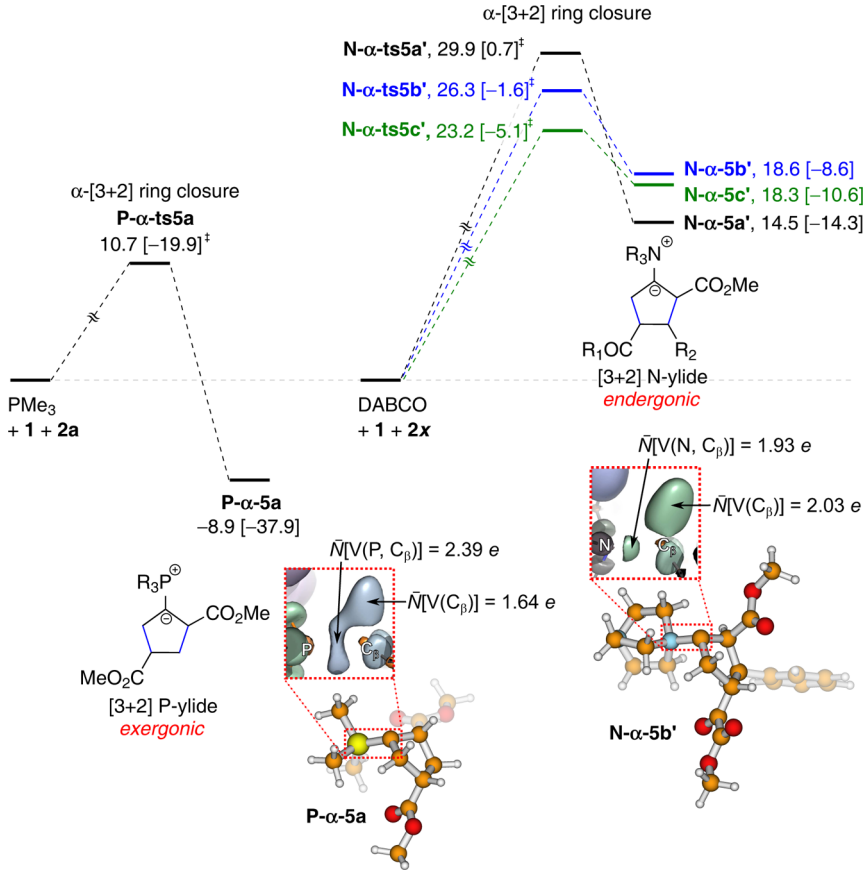

Figure 7. Activation energies of the [3 + 2] ring closure and energies of the ylides relative to Lewis bases, the allenoate **2a**, and the enones **2*x***. The isosurface of electron localization function, $\eta(\vec{r})$ = 0.8, for the [3 + 2] ylidic intermediates, **P-*α*-5a** and **N-*α*-5b′**, is shown in the dashed red boxes.

substituent in **2b** reduces the barrier along the RC-*α*-[2 + 4] pathway and stabilizes the product (Scheme 4).

The enone **2c** is more electron poor than **2b** because the phosphonate ester is a stronger electron-withdrawing group than the carboxylic ester, as quantified by the Hammett meta substituent constants[51,52] (σ_{COOMe} = 0.37, $\sigma_{PO(OMe)_2}$ = 0.45). This difference in electron deficiency is reflected in the computational result that the barriers along any pathway for **2c** are always lower than those for **2b** (Table 1). The barriers for the RC reaction and the *γ*-[2 + 4] cycloaddition are 20.8 and 16.8 kcal mol^{-1} for enone **2c**. The addition of the DABCO molecule to the allenoate (I → II, 21.9 kcal mol^{-1}) is the rate-determining step in the overall reactions with enone **2c**.

The calculated barriers show that electron-rich substituents on the enone are likely to drag the reaction path from the *γ*-[2 + 4] cycloaddition to the RC pathway. In the case of **2a**, the calculations indicate that the RC path is dominant as well as that the RC-*α*-[2 + 4] annulation is unlikely due to the high barrier. On the contrary, the *γ*-[2 + 4] cycloaddition is dominant over the RC-*α*-[2 + 4] reaction in the case of enone **2b**. Both results for **2a** and **2b** agree with the experimental observation.[19,22] However, in the case of enone **2c** calculations show that the *γ*-[2 + 4] cycloaddition (II → V, $\Delta G^{\ddagger}$ = 16.8 kcal mol^{-1}) is kinetically more favorable than the RC-*α*-[2 + 4] pathway (II → III → IV, $\Delta G^{\ddagger}$ = 20.8 kcal mol^{-1}), which contradicts the observation of the RC-*α*-[2 + 4] product as a major product in experiments. Considering that the RC-*α*-[2 + 4] product (***α*-H6c**) is 4.1 kcal mol^{-1} more stable than the *γ*-[2 + 4] product ***γ*−6c′** and that the rate determining step is the addition of DABCO to allenoate ($\Delta G^{\ddagger}$ = 21.9 kcal mol^{-1}) in the two overall *γ*-[2 + 4] cycloaddition and the RC-*α*-[2 + 4] reaction, it is reasonable to conjecture that the thermodynamic effect plays an important role for reactions with enone **2c**. The quantum calculations reveal a significant substituent effect for the DABCO catalysis which has not been observed in the [3 + 2] cyclization catalyzed by phosphines.[10,13,15,53]

3.4. Stability of [3 + 2] Phosphorus− and Ammonium−Ylides. The stability of [3 + 2] phosphorus− and ammonium−ylides is analyzed to examine the fact that the [3 + 2] cycloaddition of allenoates and enones is not catalyzed by amines but by phosphines. The ylidic intermediates **P-*α*-5a**/**N-*α*-5*x*′**, which directly lead to the formation of the cyclopentene products, play central roles to the catalytic effect on the [3 + 2] cycloaddition.

The release of the catalyst is initialized by a proton transfer in the [3 + 2] intermediates **P-*α*-5a** and **N-*α*-5b′**. While the formation of **P-*α*-5a** is exergonic (ΔG = −8.9 kcal mol^{-1}), the formation of **N-*α*-5b′** is endergonic (ΔG = 18.6 kcal mol^{-1}). The difference of stability can be linked to the nature of the P−C$_\beta$ and N−C$_\beta$ bonds despite of their structural similarity. The influence of the enone substitution is of lesser importance for the stability of the formation of the ylides, as shown in Figure 7, since the ammonium ylides are endergonic by 14 to 19 kcal mol^{-1} in the cases of **2a**, **2b** and **2c**.

Figure 7 shows the isosurface of the electron localization function (ELF) at $\eta(\vec{r})$ = 0.8. The high value of the basin population of the P−C$_\beta$ bond ($\bar{N}$[V(P, C$_\beta$)] = 2.39 e) indicates that the P−C$_\beta$ bond is stronger than the corresponding N−C$_\beta$ bond ($\bar{N}$[V(N, C$_\beta$)] = 1.93 e) for amine catalysis. The lone pair

dx.doi.org/10.1021/jo402609v | J. Org. Chem. 2014, 79, 1700−1711

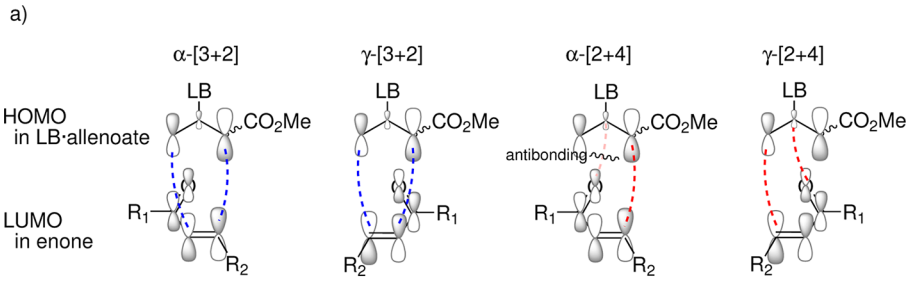

The highest barriers ($\Delta G^{\ddagger}$ in kcal mol^{-1}) for the four cyclizations

	α-[3+2]	γ-[3+2]	α-[2+4]	γ-[2+4]
P catalysis				
2a	10.8	13.8	37.8	15.6
N catalysis				
2a	15.6	14.9	32.8	17.4
2b	12.0	10.7	16.9	4.5
2c	8.9	7.4	16.7	2.5

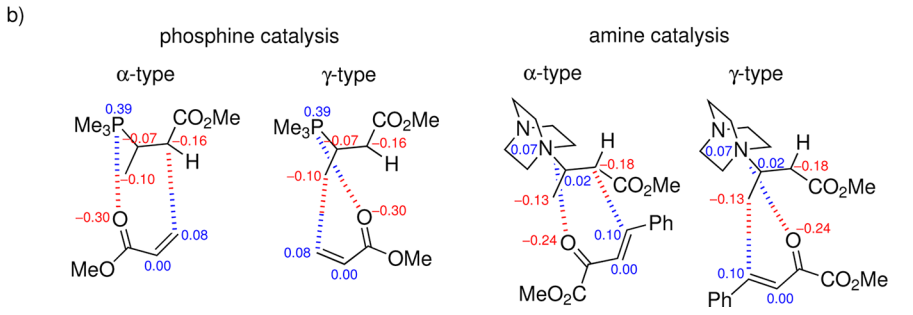

Figure 8. (a) Frontier orbital interaction in the α-[3 + 2], γ-[3 + 2], α-[2 + 4], and γ-[2 + 4] cyclizations. The table lists the highest barriers for reactions with the two catalysts. The step with the highest barrier of the cyclization can be either the initial Michael addition (marked in green) or the ring closure (marked in brown). The values for $\Delta G^{\ddagger}$ are relative to **P-c3**/**N-c3′** and ***2x*** infinitely separated from each other in toluene. (b) Electrostatic interaction between the adducts and the enones in the PMe_3- and DABCO-catalyzed cyclizations. Selected Hirshfeld atomic charges with adjacent hydrogen atoms summed to heavy atoms are given.

of the carbanion is represented by the $\bar{N}[V(C_\beta)]$ basin. In the case of phosphine catalysis, the basin overlap of the $\bar{N}[V(P, C_\beta)]$ and $\bar{N}[V(C_\beta)]$ indicating a stronger delocalization of the electrons involved. The fact that there is hardly any overlap for the amine catalysis reveals that the P−C_β bond is stronger than its N−C_β analogue and hence the phosphorus-ylide is more stable than the ammonium−ylide. The ELF information further suggests more covalent interactions in the phosphorus−ylide caused by electron donation from the carbanion while a more ionic system is observed for the ammonium-ylide.

The Hammond's postulate predicts a lower barrier for the more exothermic reaction.[54] The more stable [3 + 2] ylide (ΔG: −8.9 kcal mol^{-1}) is linked to a lower ring-closure barrier ($\Delta G^{\ddagger}$: 10.7 kcal mol^{-1}) while the less stable ammonium−ylide is linked to a higher activation energy for the [3 + 2] ring closure. For example, the formation of **N-*α*-5b′** (ΔG: 18.6 kcal mol^{-1}) goes through a transition state **N-*α*-ts5b′** with a high activation energy of 26.3 kcal mol^{-1}.

The ELF calculations show that the P−C_β ylidic bond is stronger than the N−C_β one, which correlates with the previous calculations that the formation of the P-ylide is exergonic while the formation of the N-ylide is endergonic. In conclusion, the absence of a [3 + 2] cycloaddition with amine catalysts in experiments is most likely due to the inability of amine bases to stabilize the ylidic N−C_β bond necessary for the formation of the [3 + 2] ammonium-ylidic intermediate.

3.5. FMO Analysis. A frontier molecular orbital (FMO) analysis was performed to analyze the regioselectivity of the [3 + 2] and [2 + 4] cycloadditions (Figure 8a). **P-c3** was chosen to represent phosphine catalysis and **N-c3′** for amine catalysis. There is one antibonding interaction between C_β and the enone oxygen atom in the α-[2 + 4] cycloaddition, whereas there are only bonding interactions for the remaining three cyclization pathways. Consequently, the highest barriers for the ring closure are found along the α-[2 + 4] pathway as shown in Figure 3 and Table 1, which corroborates the argument that the α-[2 + 4] pyran is formed via the RC product.

The FMO analysis shows two bonding interactions along the bonds to be formed in both [3 + 2] cycloadditions. The FMO overlaps in the α-[3 + 2] and γ-[3 + 2] cycloadditions are similar. The α-[3 + 2] or γ-[3 + 2] preference depends on the catalyst: the α-[3 + 2] cycloaddition is more favorable than the γ-[3 + 2] one in phosphine catalysis and vice versa in amine catalysis (Figure 3 and Table 1).

There is a weak bonding interaction between C_β and the enone oxygen atom for the γ-[2 + 4] cycloaddition. The contribution of the oxygen atom to the LUMO of the enone depends strongly on the substitution of the enone and so does the extent of the bonding FMO interactions along the forming C_β−O bond (detailed information in Figure S24, Supporting Information). This dependence of the FMO interaction on the substitution is reflected in different barrier heights for the three enones **2a**, **2b**, and **2c**. Electron-withdrawing substituents on the enone

dx.doi.org/10.1021/jo402609v | J. Org. Chem. 2014, 79, 1700−1711

(**2b** and **2c**) reduce the energy difference between the adduct HOMO and the enone LUMO, which results in stronger interactions between the frontier orbitals and a lower barrier. Furthermore, the contribution of the C_β atom to the enone LUMO decreases by approximately 40% while the contribution from the oxygen atom to the same orbital increases by approximately 20% (Figure S24, Supporting Information). The increase in the contribution form the oxygen atom favors the γ-[2 + 4] cycloaddition while the decrease in the carbon contribution disfavors the [3 + 2] cycloaddition. The large diminution in barrier height between 14 to 16 kcal mol^{-1} for the γ-[2 + 4] cycloaddition reflects the cooperation between a decreasing HOMO−LUMO gap and the change on orbital contributions on the oxygen atom (Figure 8a). The reduction in barrier height for the [3 + 2] cycloaddition is smaller (4 to 8 kcal mol^{-1}), because the gain from the decreasing HOMO−LUMO gap is offset by the unfavorable change in orbital contributions from the C_α atom of the enone.

The accompanying Coulomb interactions are summarized in Figure 8b. The Hirshfeld charge analysis always assigns the largest negative charge to the oxygen atom of the enone. Its counterpart is the large positive partial charge on the P atom in the case of phosphine catalysis. This electrostatic interaction accounts for the short P···O_{enone} distances of 2.86 and 2.62 Å in **P-*α*-4a** and **P-*γ*-4a**. For amines, it is less clear as positive charges of C_β (q_C = +0.02 e) and the bonding DABCO nitrogen atom (q_N = +0.07 e) are similar. The Coulomb attraction between C_β−O is likely to benefit the formation of a C_β−O bond during the [2 + 4] cyclization.

4. CONCLUSIONS

This study explains the origin of different reactivity between phosphine and amine catalysts and the substituent effect of the enone in amine catalysis. The phosphine- and amine-catalyzed cycloaddition of allenoates and enones yields two different cyclic products: [3 + 2] cyclopentenes and [2 + 4] dihydropyrans/pyrans. Calculations indicate that phosphine catalysts favor the [3 + 2] cycloaddition over the [2 + 4] one. The preference of the [3 + 2] cycloaddition is attributed to the exergonic formation of a stable phosphorus−ylide. The following proton transfer can be achieved via a self-tautomerization or a water-assisted mechanism. The initial addition of the phosphines to the allenoate is the rate-determining step in the overall [3 + 2] cycloaddition.

Amine catalysts do not support the formation of ammonium−ylides and hence do not facilitate the production of [3 + 2] cyclopentenes. The Rauhut−Currier (RC) pathway and the γ-[2 + 4] cycloaddition compete with each other when amines are used as catalysts, and the substitution on the enone determines the reaction pathway. Water effectively helps the proton transfer of the RC pathway. An electron-rich enone (**2a**) exclusively yields acyclic RC products (α-substituted allenoates) since a ring-closing step in any of the cycloadditions is kinetically disfavored. Electron-poor enones (**2b** and **2c**) lead to the γ-[2 + 4] cycloadditions while α-[2 + 4] pyrans are further formed from the RC product in an additional annulation (RC-α-[2 + 4]). For the electron-poor enone (**2b**), the γ-[2 + 4] cycloaddition is kinetically dominant over the RC-α-[2 + 4] reaction. Conversely, the electron-poorer enone (**2c**) is prone to the RC-α-[2 + 4] pathway under thermodynamical control since the activation energies for both the γ-[2 + 4] and the RC-α-[2 + 4] pathways are lower than that for the addition of DABCO to the allenoate. Moreover, more HOMO−LUMO interaction along the γ-[2 + 4] cycloaddition favors the formation of the *E*-dihydropyran over the *Z*-isomer. FMO analysis shows that the α-[2 + 4] cycloaddition is the least favorable, and the preference between [3 + 2] and γ-[2 + 4] cycloadditions depends on the catalyst as well as the substituent of the enone. The computational analysis reveals a possible path to the α-[2 + 4] cycloadduct via an intermediate Rauhut-Currier reaction, which is much more favorable than the direct α-[2 + 4] cycloaddition. We hope that the mechanistic detail provided by this study will lead to development of better phosphine and amine catalysts for the synthesis of complex natural products.

■ ASSOCIATED CONTENT

Supporting Information

Detailed calculations for all reaction pathways. This material is available free of charge via the Internet at http://pubs.acs.org.

■ AUTHOR INFORMATION

Corresponding Author

*E-mail: chyu@oxygen.chem.nthu.edu.tw.

Notes

The authors declare no competing financial interest.

■ ACKNOWLEDGMENTS

This work is supported by the National Science Council of the Republic of China under Grant No. NSC 100-2113-M-007-008-MY3. T.L. acknowledges a university research associateship from the National Tsing Hua University.

■ REFERENCES

(1) Krause, N., Hashmi, A. S. K., Eds. *Modern Allene Chemistry*; Wiley-VCH: Weinheim, 2004.
(2) Ma, S. *Chem. Rev.* **2005**, *105*, 2829−72.
(3) Yu, S.; Ma, S. *Angew. Chem., Int. Ed.* **2012**, 3074−3112.
(4) López, F.; Mascarenas, J. L. *Chem.—Eur. J.* **2011**, *17*, 418−28.
(5) Cowen, B. J.; Miller, S. J. *Chem. Soc. Rev.* **2009**, *58*, 3102−16.
(6) Zhang, C.; Lu, X. *J. Org. Chem.* **1995**, *60*, 2906−2908.
(7) Zhu, G.; Chen, Z.; Jiang, Q.; Xiao, D.; Cao, P.; Zhang, X. *J. Am. Chem. Soc.* **1997**, *119*, 3836−3837.
(8) Xu, Z.; Lu, X. *Tetrahedron Lett.* **1997**, *58*, 3461−3464.
(9) Xu, Z.; Lu, X. *J. Org. Chem.* **1998**, *65*, 5031−5041.
(10) Wilson, J. E.; Fu, G. C. *Angew. Chem., Int. Ed.* **2006**, *45*, 1426−9.
(11) Pinto, N.; Neel, M.; Panossian, A.; Retailleau, P.; Frison, G.; Voituriez, A.; Marinetti, A. *Chem.—Eur. J.* **2010**, *16*, 1033−45.
(12) Cowen, B. J.; Saunders, L. B.; Miller, S. J. *J. Am. Chem. Soc.* **2009**, *131*, 6105−7.
(13) Fujiwara, Y.; Fu, G. C. *J. Am. Chem. Soc.* **2011**, *133*, 12293−7.
(14) Liang, Y.; Liu, S.; Xia, Y.; Li, Y.; Yu, Z.-X. *Chem.—Eur. J.* **2008**, *14*, 4361−73.
(15) Zhang, X.-C.; Cao, S.-H.; Wei, Y.; Shi, M. *Chem. Commun.* **2011**, *47*, 1548−50.
(16) Chen, X.-y.; Wen, M.-w.; Ye, S.; Wang, Z.-x. *Org. Lett.* **2011**, *13*, 1138−41.
(17) Wang, X.; Fang, T.; Tong, X. *Angew. Chem., Int. Ed.* **2011**, *50*, 5361−4.
(18) Ashtekar, K. D.; Staples, R. J.; Borhan, B. *Org. Lett.* **2011**, *13*, 5732−5.
(19) Pei, C.-K.; Wu, L.; Lian, Z.; Shi, M. *Org. Biomol. Chem.* **2012**, *10*, 171−80.
(20) Pei, C.-K.; Jiang, Y.; Shi, M. *Org. Biomol. Chem.* **2012**, *10*, 4355−61.
(21) Zhang, X.-C.; Cao, S.-H.; Wei, Y.; Shi, M. *Org. Lett.* **2011**, *13*, 1142−5.
(22) Pei, C.-K.; Jiang, Y.; Wei, Y.; Shi, M. *Angew. Chem., Int. Ed.* **2012**, 11328−11332.
(23) Pei, C.-K.; Shi, M. *Chem.—Eur. J.* **2012**, *18*, 6712−6.
(24) Evans, C. A.; Miller, S. J. *J. Am. Chem. Soc.* **2003**, *125*, 12394−5.

(25) Evans, C. a.; Cowen, B. J.; Miller, S. J. *Tetrahedron* **2005**, *61*, 6309−6314.
(26) Li, C.; Zhang, Q.; Tong, X. *Chem. Commun.* **2010**, *46*, 7828−30.
(27) Li, K.; Hu, J.; Liu, H.; Tong, X. *Chem. Commun.* **2012**, *48*, 2900−2.
(28) Zhao, Y.; Truhlar, D. G. *Theor. Chem. Acc.* **2007**, *120*, 215−241.
(29) Raghavachari, K.; Trucks, G. W.; Pople, J. A.; Head-Gordon, M. *Chem. Phys. Lett.* **1989**, *157*, 479−483.
(30) Frisch, M. J. et al. Gaussian 09 Revision A.1; Gaussian, Inc.: Wallingford, CT, 2009.
(31) Barone, V.; Cossi, M.; Tomasi, J. *J. Comput. Chem.* **1998**, *19*, 404.
(32) CanceÌÀs, E.; Mennucci, B.; Tomasi, J. *J. Chem. Phys.* **1997**, *107*, 3032.
(33) Cossi, M.; Barone, V.; Cammi, R.; Tomasi, J. *Chem. Phys. Lett.* **1996**, *255*, 327−335.
(34) Becke, A. D.; Edgecombe, K. E. *J. Chem. Phys.* **1990**, *92*, 5397.
(35) Noury, S.; Krokidis, X.; Fuster, F.; Silvi, B. *Comput. Chem.* **1999**, *25*, 597−604.
(36) Gandhi, R. P.; Ishar, M. P. S. *Magn. Reson. Chem.* **1991**, *29*, 671−674.
(37) Hirshfeld, F. L. *Theoret. Chim. Acta* **1977**, *44*, 129−138.
(38) Buono, G.; Llinas, J. R. *J. Am. Chem. Soc.* **1981**, *103*, 4532−4540.
(39) Zhao, Y.; Ng, H. T.; Peverati, R.; Truhlar, D. G. *J. Chem. Theory Comput.* **2012**, *8*, 2824−2834.
(40) Xia, Y.; Liang, Y.; Chen, Y.; Wang, M.; Jiao, L.; Huang, F.; Liu, S.; Li, Y.; Yu, Z.-X. *J. Am. Chem. Soc.* **2007**, *129*, 3470−1.
(41) Kumar, K.; Kapur, A.; Ishar, M. P. S. *Org. Lett.* **2000**, *2*, 787−789.
(42) Zhu, X.-F.; Henry, C. E.; Wang, J.; Dudding, T.; Kwon, O. *Org. Lett.* **2005**, *7*, 1387−90.
(43) Cantillo, D.; Kappe, C. O. *J. Org. Chem.* **2010**, *75*, 8615−26.
(44) Aggarwal, V. K.; Fulford, S. Y.; Lloyd-Jones, G. C. *Angew. Chem., Int. Ed.* **2005**, *44*, 1706−8.
(45) Roy, D.; Sunoj, R. B. *Chem.—Eur. J.* **2008**, *14*, 10530−4.
(46) Jørgensen, K. *Angew. Chem., Int. Ed.* **2000**, *59*, 3558−3588.
(47) Kitagaki, S.; Kawamura, T.; Shibata, D.; Mukai, C. *Tetrahedron* **2008**, *64*, 11086−11095.
(48) Mukai, C.; Kuroda, N.; Ukon, R.; Itoh, R. *J. Org. Chem.* **2005**, *70*, 6282−90.
(49) Mukai, C.; Ohta, M.; Yamashita, H.; Kitagaki, S. *J. Org. Chem.* **2004**, *69*, 6867−73.
(50) Mukai, C.; Yamashita, H.; Hanaoka, M. *Org. Lett.* **2001**, *3*, 3385−3387.
(51) Hansch, C.; Leo, A.; Taft, R. W. *Chem. Rev.* **1991**, *91*, 165−195.
(52) Hammett, L. P. *Chem. Rev.* **1935**, *17*, 125−136.
(53) Schuler, M.; Voituriez, A.; Marinetti, A. *Tetrahedron: Asymmetry* **2010**, *21*, 1569−1573.
(54) Hammond, S. *J. Am. Chem. Soc.* **1953**, *77*, 334−338.